Insertion of Lipidated Ras Proteins into Lipid Monolayers Studied by Infrared Reflection Absorption Spectroscopy (IRRAS)

Annette Meister,* Chiara Nicolini,† Herbert Waldmann,‡ Jürgen Kuhlmann,§ Andreas Kerth,* Roland Winter,† and Alfred Blume*

*Institut für Physikalische Chemie, Martin-Luther-Universität Halle-Wittenberg, Halle, Germany; †Fachbereich Chemie, Physikalische Chemie I – Biophysikalische Chemie, Universität Dortmund, Dortmund, Germany; and ‡Abteilung für Chemische Biologie, and §Abteilung für Strukturelle Biologie, Max-Planck-Institut für Molekulare Physiologie, Dortmund, Germany

ABSTRACT Ras proteins have to be associated with the inner leaflet of the plasma membrane to perform their signaling functions. This membrane targeting and binding is controlled by post-translational covalent attachment of farnesyl and palmitoyl chains to cysteines in the membrane anchor region of the N- and H-Ras isoforms. Two N-Ras lipoproteins were investigated, namely a farnesylated and hexadecylated protein, presenting the natural hydrophobic modifications and a doubly hexadecylated construct, respectively. The proteins are surface active and form a Gibbs monolayer at the air-D_2O interface. The contours of the amide-I bands were analyzed using infrared reflection absorption spectroscopy (IRRAS). Langmuir monolayers of a mixture of POPC, brain sphingomyelin, and cholesterol were used as half of a model biomembrane to study the insertion of these N-Ras proteins. They insert with their hydrophobic anchors into lipid monolayers but at higher surface pressures (30 mN/m); the farnesylated and hexadecylated protein desorbs completely from the monolayer, whereas the doubly hexadecylated protein remains incorporated. During the insertion process, changes in the orientation of the protein secondary structure were detected by comparison with simulated IRRA spectra, based on the information on the relative orientation of the secondary structure elements from the protein crystal structure data.

INTRODUCTION

Ras proteins are GTPases involved in the regulation of cell differentiation, mitosis, growth control, and cell cycle regulation, acting as molecular switches shuttling between active GTP-bound and inactive GDP-bound states (1,2). Three members of the Ras family, H-Ras, N-Ras, and K-Ras, are expressed in mammalian cells, where they generate distinct signal outputs (3,4). To perform their physiological functions, plasma membrane-associated Ras proteins require a series of posttranslational processing steps, starting with farnesylation of the C-terminal cysteine (5). H- and N-Ras proteins are also palmitoylated on additional cysteine residues in the C-terminus (6). Both palmitoylation and farnesylation are necessary for plasma membrane association of H- and N-Ras (7–9). The partitioning of the lipidated C-terminus of N-Ras into lipid model membranes has been the subject of a series of investigations applying various techniques, such as solid-state NMR, neutron diffraction, FTIR spectroscopy, fluorescence microscopy, and two-photon excitation fluorescence microscopy (10–14). In this context the corresponding Ras lipoproteins became accessible by a semisynthetic approach combining a bacterially expressed protein core with a chemically generated lipopeptide (15). Recently, the insertion of the completely lipidated N-Ras protein into heterogeneous lipid bilayer systems was described by two-photon excitation fluorescence microscopy on giant unilamellar vesicles and atomic force microscopy (16). The results provide direct evidence that the partitioning of the farnesylated/hexadecylated protein occurs preferentially into liquid-disordered lipid domains.

This work focuses on interactions of two doubly lipidated N-Ras proteins with lipid monolayers at the air-D_2O interface. The insertion behavior of the farnesylated and hexadecylated as well as of the doubly-hexadecylated protein into a monolayer of POPC, brain sphingomyelin, and cholesterol was followed by infrared reflection absorption spectroscopy (IRRAS). In recent years, the use of Langmuir monolayers (17–19) and techniques such as grazing incidence x-ray diffraction (20–23), and neutron and x-ray reflectivity (24,25) as well as IRRAS (26–31) have become common methods for the study of lipid-protein interactions. Representing one-half of a biological membrane, lipid monolayers can mimic membrane surfaces and provide an ideal model system for peripheral adsorption or insertion of proteins into only one monolayer of a lipid bilayer. The changes in the lipid structure as well as the secondary peptide or protein structure and its orientation can be followed by IRRAS at desired pH, buffer, and ionic strength. The aim of this study is to discuss orientational changes of the protein secondary structure and the role of the farnesyl and hexadecyl anchor of N-Ras proteins during the insertion into liquid-expanded monolayers of a model lipid mixture.

Submitted March 10, 2006, and accepted for publication May 15, 2006.

Address reprint requests to Alfred Blume, Institute of Physical Chemistry, Martin-Luther-University Halle-Wittenberg, Muehlpforte 1, 06108 Halle/Saale, Germany. Tel.: 49-345-552-5850; Fax: 49-345-552-7157; E-mail: alfred.blume@chemie.uni-halle.de.

0006-3495/06/08/1388/14 $2.00

doi: 10.1529/biophysj.106.084624

MATERIALS AND METHODS

Materials

1-Palmitoyl-2-oleoyl-*sn*-glycero-3-phosphocholine (POPC) and brain sphingomyelin (BSM) were purchased from Avanti Polar Lipids (Birmingham, AL) and cholesterol (Chol) from Sigma-Aldrich (Deisenhofen, Germany). The doubly-lipidated proteins HFar-N-Ras (Fig. 1 *A*) and DH-N-Ras (Fig. 1 *B*) were synthesized as described previously (32,33). In these proteins the hydrolysis labile acylthioester of the palmitoyl function is replaced by a stable hexadecyl thioether to prevent spontaneous decomposition during the measurements. We have shown that semisynthetic Ras lipoproteins with a maleimido-bridged C-terminus carrying a farnesyl and carboxymethyl moiety show a qualitatively identical binding to an artificial membrane system built on a BIAcore sensor chip, as an in vitro farnesylated Ras protein (15). Biological activity of semisynthetic Ras lipoproteins has been proven for several constructs that carry an oncogenic mutation (G12V) in the protein core. Here, RasG12V lipoproteins carrying a farnesyl thioether and a carboxymethylation at the C-terminus and either a hexadecylated or palmitoylated cysteine in the lipopeptide moiety are capable to induce differentiation of PC12 cells after microinjection that indicates functionality of the Ras signaling pathway (15). The same has been demonstrated with a palmitoylated Ras lipoprotein whose carboxymethyl-group has been replaced by a BODIPY-FL fluorophore (32). Chloroform and methanol were purchased from Roth (Karlsruhe, Germany) and sodium chloride from Sigma-Aldrich. For all film balance measurements D_2O from Isotec (Miamisburg, OH) was used.

Methods

Protein adsorption

Adsorption experiments were performed with a circular homebuilt Teflon trough with a total area of 7.07 cm^2, and a volume of 11.15 ml. Protein solutions (0.279 mM) were injected with a Hamilton syringe through the Teflon jacket just above the bottom of the trough. A tiny magnet stirred the subphase to assure a homogeneous distribution of the protein. The surface pressure was measured by the Wilhelmy method, using a filter paper as Wilhelmy plate. The temperature of the D_2O subphase containing 100 mM NaCl was maintained at 20 $\pm$ 0.5°C, and a Plexiglas hood covered the trough to minimize evaporation of D_2O.

Lipid monolayer preparation

All experiments were performed with a Wilhelmy film balance (Riegler & Kirstein, Berlin, Germany) using a filter paper as Wilhelmy plate. Two Teflon troughs of different size (300 $\times$ 60 $\times$ 3 mm^3 and 60 $\times$ 60 $\times$ 3 mm^3 for the reference trough) were linked by three small water-filled bores to ensure equal height of the air-D_2O interface in both troughs. The temperature of the subphase was maintained at 20 $\pm$ 0.5°C. The movement of the Teflon barriers of the larger sample trough was computer-controlled. Measurements were performed in the large trough, the smaller one usually serving as reference trough. A Plexiglas hood covered both troughs to minimize evaporation of D_2O. Both troughs were filled with 100 mM NaCl in D_2O. Monolayers composed of POPC/BSM/Chol (50:25:25 mol %) were formed by directly spreading the lipid solution (~1 mM) in a mixture of chloroform and methanol (3:1) onto the subphase. After an equilibration period of at least 15 min, the π-A isotherms were recorded at a constant compression speed of 2 $Å^2$ $molecule^{-1}$ min^{-1}.

IRRAS

Infrared spectra were recorded with an Equinox 55 FT-IR spectrometer (Bruker, Karlsruhe, Germany) connected to an XA 511 reflection attachment (Bruker) with an external narrow band MCT detector using the trough system described above. The IR beam is focused by several mirrors onto the water surface and different angles of incidence can be adjusted. A computer controlled rotating KRS-5 polarizer (>98% degree of polarization) was used to generate parallel and perpendicularly polarized light. The trough system was positioned on a moveable platform to be able to shuttle between the sample and the reference trough. This shuttle technique diminishes the spectral interferences due to the water vapor absorption in the light beam (34).

Protein adsorption experiments at the air-D_2O interface were performed in the small reference trough by injection of a concentrated protein solution (0.279 mM) into the subphase. Lipid-protein interactions were studied either at constant surface pressure in the large trough or at constant surface area in the small trough. The lipid monolayer films in the large trough were compressed to a desired surface pressure, the barriers were then stopped, and the acquisition of the IRRAS spectra started before the injection of the protein into the subphase. In these experiments, the angle of the incident infrared beam with respect to the normal of the D_2O surface was 40° and parallel polarized radiation was used. After reaching a constant surface

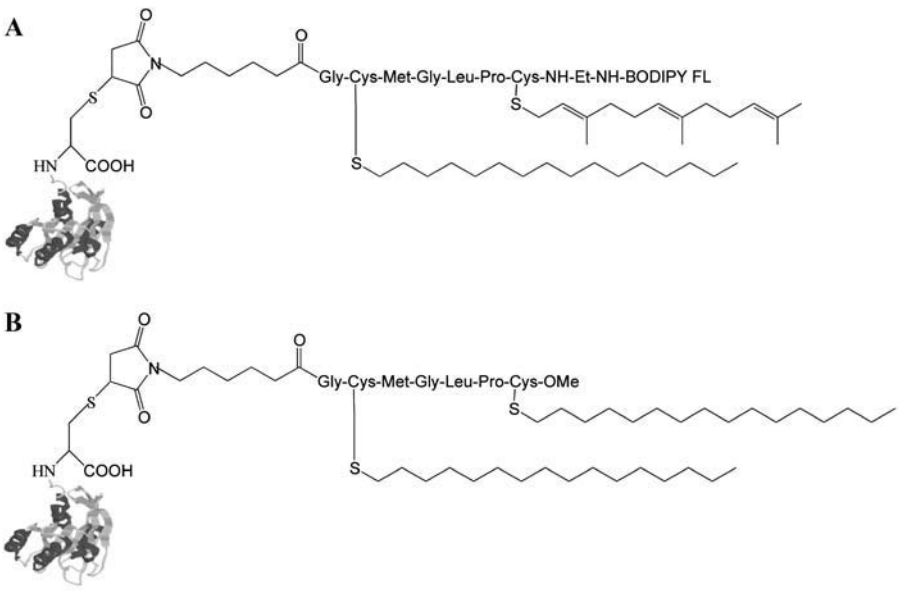

FIGURE 1 Structures of the semisynthetic HFar-N-Ras (*A*) and DH-N-Ras (*B*) proteins.

pressure, measurements at different angles using parallel and perpendicularly polarized light were performed.

For experiments at constant surface area, the lipid mixture was spread onto the air-D_2O interface of the small trough up to the desired surface pressure (10 mN/m). The high methylene stretching band frequencies throughout the experiments indicate largely disordered monolayers and assume a good spreading behavior, independent of the preparation of the lipid monolayer. Perpendicularly polarized light with an angle of incidence of 40° was used for the recording of the IRRA spectra. For measurements at different angles, parallel and perpendicular polarized radiation was used. All spectra were recorded at a spectral resolution of 8 cm^{-1} using Blackman-Harris-4-Term apodization and a zero filling factor of 2. For each spectrum, 2000 or 4000 scans were co-added over a total acquisition time of ~6–9 min. The single-beam reflectance spectrum of the reference trough surface was ratioed as background to the single beam reflectance spectrum of the monolayer on the sample trough to calculate the reflection absorption spectrum as $-\log(R/R_0)$. Peak positions were determined by the standard peak picking method (interpolation), supplied by the Bruker software (OPUS). Spectral calculations were performed using a Visual Basic program (23) with an implementation of the formalism published by Mendelsohn et al. (35) and Flach et al. (36).

Molecular modeling

Models were developed using the Materials Studio software 4.0 (Accelrys, San Diego, CA). Structural data of a truncated H-Ras protein P21 were obtained from the Brookhaven data bank (PDB entry 121p) (37).

RESULTS AND DISCUSSION

Protein adsorption at the air-D_2O interface

We first studied the adsorption of the HFar-N-Ras protein (Fig. 1 *A*) at the air-D_2O interface as a function of protein concentration (Fig. 2). Only for a protein concentration of 200 nM and higher, the surface pressure started to increase immediately after injection of the protein solution into the subphase, indicating the protein surface activity. For lower concentrations, a lag time was observed before a surface pressure increase occurred. A similar behavior was reported for the GM2-activator protein (17) and KLAL peptides (38). It is known that many proteins are easily adsorbed on Teflon surfaces, due to hydrophobic side chains or surfaces. Therefore the observed effect is probably due to the initial adsorption of the protein to the Teflon walls of the trough, resulting in an actual subphase concentration that is lower than the calculated one. The N-Ras protein has a molecular mass of 21.7 kDa. Assuming a certain orientation of the protein with respect to the Teflon surface, an area of ~1700 $Å^2$/molecule could be in contact with this interface (estimated from structural data from the Brookhaven data bank of proteins). Because the Teflon surface of our trough amounts to ~10 cm^2, 60×10^{12} molecules of the protein would be adsorbed at this surface assuming a monomolecular coverage of the Teflon trough walls. This number corresponds to 0.1 nMol or a calculated concentration of ~9 nM. This means that under the assumption of a fast adsorption to the Teflon, essentially no protein would be in the subphase or the surface up to this concentration, so that no measurable surface pressure increase would be observed. At higher protein concentrations, the real subphase concentration would then be ~9 nM lower due to the adsorption to the Teflon walls. The real situation is probably not that extreme, but the Teflon adsorption can easily explain the observed lag times in the increase in surface pressure. The assumption of Teflon adsorption is supported by the observation that the Teflon surface can be wetted by water when the trough has been emptied for cleaning. Many authors have reported adsorption of proteins to Teflon surfaces with amounts of up to 4 mg/m^2, when saturation is reached. The values calculated above correspond to a saturation value of ~2 mg/m^2, and are well within the range reported for other proteins (39).

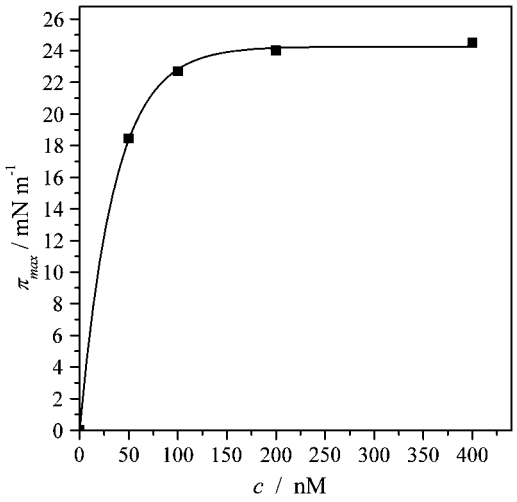

FIGURE 2 Maximal surface pressure π_{max} as a function of the protein concentration for the doubly-lipidated HFar-N-Ras protein (c = 50, 100, 200, 400 nM, T = 20°C, in 100 mM NaCl, D_2O). The value π_{max} was obtained 6 h after the protein injection in the small circular trough, equipped with a magnetic stirrer (see Materials and Methods).

Fig. 2 shows the maximal surface pressure as a function of the protein concentration in the subphase. For the HFar-N-Ras, lipidated with farnesyl and hexadecyl anchors, the maximum value of π approaches 24 mN m^{-1} at a protein concentration of 200 nM. This value seems to be close to the saturation value and is related to the surface activity of the protein, i.e., the change in free energy due to the adsorption at the air-D_2O interface. For the GM2-activator protein this value is 21 mN/m (17), lactoglobulin approaches a surface pressure of 20 mN/m (40), and KLAL peptides 20 to 21.5 mN/m (38). The N-Ras protein is therefore even slightly more surface-active than these other proteins or peptides, probably because it is doubly lipidated.

The adsorption kinetics of the two different N-Ras proteins at the air-D_2O interface were also investigated by IRRAS using a fixed protein concentration in the trough of 200 nM (Fig. 3, *A* and *C*). HFar-N-Ras shows the expected adsorption behavior in that a smooth continuous increase in surface pressure is observed. After 22 h, the surface pressure reaches a plateau value of 19.5 mN/m. For DH-N-Ras with

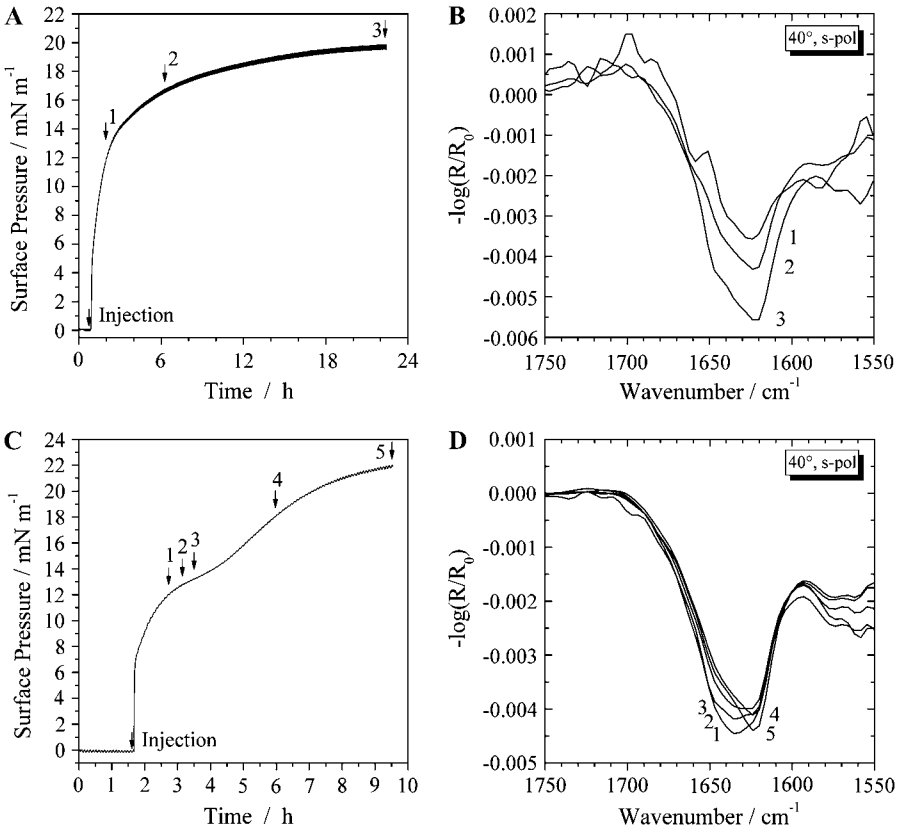

FIGURE 3 (*A*) Surface-pressure versus time-course of HFar-N-Ras films at a 200 nM protein concentration starting with the injection of the appropriate volume of the stock solution into the subphase. (*B*) IRRA spectra of the HFar-N-Ras film with the 200 nM protein concentration at the respective positions *1–3* of the surface-pressure time-curve in Fig. 1 *A*. All spectra have been recorded at an angle of incidence of 40° and with s-polarized light. (*C*) Surface-pressure versus time-course of DH-N-Ras films at a 200 nM protein concentration starting with the injection of the appropriate volume of the stock solution into the subphase. (*D*) IRRA spectra of the DH-N-Ras film with the 200 nM protein concentration at the respective positions *1–5* of the surface-pressure time-curve in Fig. 1 *C*. All spectra have been recorded at an angle of incidence of 40° and with s-polarized light.

the two hexadecyl residues, a kinetic curve indicating a stepwise adsorption is seen. After 3.5 h, a first short plateau at a surface pressure of 13 mN/m is obtained, then the surface pressure increases further and reaches after 10 h a final value at ~22 mN/m. This indicates that DH-N-Ras adsorbs nearly twice as fast as HFar-N-Ras at the air-water interface. IRRA spectra recorded at different times during the adsorption process are shown in Fig. 3, *B* and *D*.

The amide-I band of the farnesylated protein increases in intensity during the whole adsorption process (Fig. 3 *B*). The wavenumber of the band maximum shifts slightly from 1625 cm^{-1} (Fig. 3 *B*, *1*) to 1623 cm^{-1}, where it stays constant up to the end of the adsorption process (Fig. 3 *B*, *2* and *3*). This is a characteristic value for a β-sheet secondary structure; the weak band at ~1680 cm^{-1} indicative of antiparallel β-sheets is missing. This observation agrees with the x-ray structure of Ras proteins, which shows five parallel and only one antiparallel strand. Hence, our data point to a parallel orientation of the strands (41). Because of the limited sensitivity, the weak 1680 cm^{-1} band of the antiparallel strand is not detectable in the IRRA spectrum. The shoulders at 1650 cm^{-1} are indicative of α-helical secondary structure elements, which is consistent with the x-ray structure which shows 5 α-helices. The amide-II band is expected near 1450 cm^{-1} due to H-D exchange (42). Since this spectral region is obscured by the HOD bending mode at ~1460 cm^{-1}, no amide-II band could be detected.

For the protein with two hexadecyl chains, the amide-I band maximum is located at 1634 cm^{-1} at low surface pressures (Fig. 3 *D*). At the first surface pressure plateau, however, the band maximum is shifted to 1629 cm^{-1} and finally to 1623 cm^{-1} (characteristic for β-sheets) at the saturation surface pressure. We assume that the secondary structure of the Ras protein with five α-helices and six strands in one β-sheet does not change during this adsorption process, as this would be very unlikely. The amide-I band at low surface pressure is a superposition of amide-I bands at 1650 cm^{-1} and 1623 cm^{-1}, which represent the α-helical and β-sheet secondary structures in the protein. The observed band shift is therefore caused by a change in the orientation of the secondary structure elements of the protein relative to the air-D_2O interface. Although we cannot completely rule out a possible change in the overall secondary structure, we favor this interpretation. The reason is that the Ras protein is bound to the membrane by its lipid anchors, which are connected to the flexible C-terminus, thus decoupling the protein itself from its membrane-binding site. Because we essentially see no major differences between the spectra of the protein adsorbed to the surface and to a lipid monolayer (see below), we believe that the observed spectral changes are caused by changes in orientation and not by changes in the overall secondary structure. The latter would increase the amount of disordered structures, which could not be observed, however.

To elucidate possible changes in orientation of the protein from IRRAS measurements, the x-ray structure of the protein has to be known but unfortunately, no structure of N-Ras is available in the literature. The x-ray structure of the truncated H-Ras P 21 protein is shown in Fig. 4 in different possible orientations relative to the air-D_2O interface (37). The protein structure contains 166 amino acids from the N-terminus. The hypervariable region with the linker domain (14 amino acids) and the membrane anchor (10 amino acids) are not included in the crystal structure. This C-terminal region is different for N- and H-Ras but it is assumed that this does not lead to a change of the secondary structure of the rest of the protein. As the hypervariable region is not present in the published x-ray structure of H-Ras, we could only use this as the basis for our simulations. The hydrophobicity of the protein can be estimated from the different colors of the secondary structures. Whereas the hydrophobic parts (*red*) are essentially enclosed in the protein core, the hydrophilic parts (*blue*) point outside. The C-terminus where the membrane anchors are located is indicated by an arrow. Starting from a specific orientation shown in Fig. 4 *A*, the three other orientations (*B–D*) correspond to a random orientation (*B*, not shown) and two orientations (*C* and *D*) obtained by a $\pm 45°$ rotation of the protein in orientation *A* about the *x* axis. In the different orientations the α-helices and also the β-sheet substructures have different orientations with respect to the air-D_2O interface. This should result in different contributions of the α-helical and the β-sheet elements to the observed amide-I band contour. From the spectra shown in Fig. 3 a decision about the possible orientation cannot be made. More spectral information is needed using more angles of incidence and different orientation of the polarization of the incident light. We therefore performed measurements using s- and p-polarized light at different angles of incidence at surface pressure values in the pressure plateau region. For HFar-N-Ras, the surface pressure was 20 mN/m (see Fig. 5, *A* and *B*) and for DH-N-Ras, the surface pressure was slightly higher with 22 mN/m (see Fig. 5, *C* and *D*). For s-polarized light, the absolute values of the band intensity in the reflectance-absorbance spectrum increase monotonically with increasing angle of incidence and therefore do not allow us to obtain detailed information about the anisotropy of the film. The reason for this is that s-polarized light probes only the dipole moment component parallel to the surface, whereas p-polarized light probes the dipole moment components parallel and perpendicular to the surface. As a consequence of the latter, the sign of the band changes around the Brewster-angle and the resulting changes in band shape, intensity, and position allow the determination of orientations of secondary structure elements.

Determination of orientation from amide-I band simulations

The orientation of peptide secondary structures was first determined applying PM-IRRAS by Cornut et al. (43), who generated values of optical anisotropy indices of the film by taking into account the relative infrared absorptions and dichroism for the amide-I and amide-II absorptions of an α-helical secondary structure. Theoretical normalized PM-IRRA signals were calculated for an anisotropic polypeptide monolayer. When the helix axis is parallel to the interface, these simulations give a strong positive amide-I band and a weak positive amide-II band in the PM-IRRA spectra. Conversely, when the α-helix is perpendicular to the interface, a negative strong amide-I band and a strong positive amide-II band are expected. For our IRRA spectra, the signs are just the opposite by convention. In the following years, a series of investigations was performed to determine the orientation of peptides and proteins at the air-water interface and also incorporated into lipid monolayers (44). In most cases the PM-IRRAS measurements were performed only at a constant angle of incidence of $\sim 75°$ due to technical reasons and the value of the amide-I/amide-II ratio was taken to determine the orientation of the secondary structure units (45–48).

A different approach was used by Gericke et al. (49), who compared experimental and simulated IRRA spectra at different angles of the incident p- and s-polarized light. From the position of the amide-I bands and their intensities, they were able to calculate the helix tilt angle for the pulmonary surfactant-specific protein SP-C. The same type of analysis was used by Kerth et al. (38) for the determination of the secondary structure of KLAL, an amphipathic peptide, and its orientation at the air-water interface and also for the orientation of the amyloid β (1–40) peptide (23). The authors

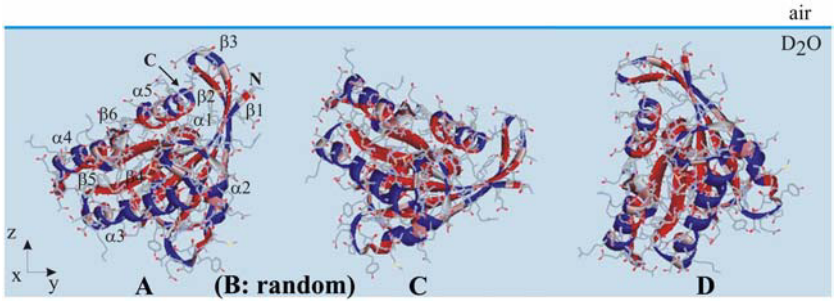

FIGURE 4 (*A*) Assumed orientation of truncated H-Ras P21 protein (PDB entry 121p) (37) relative to the normal of the air-D_2O interface. (*B–D*) indicate other orientations corresponding to a random orientation *B* (not shown) and two orientations (*C*,*D*) obtained by a $\pm$ 45° rotation of the protein in orientation *A* around the *x* axis. The hydrophobic and hydrophilic parts of the protein are indicated in red and blue, respectively. The position of the truncated C-terminus with the lipidation sites is indicated by the arrow.

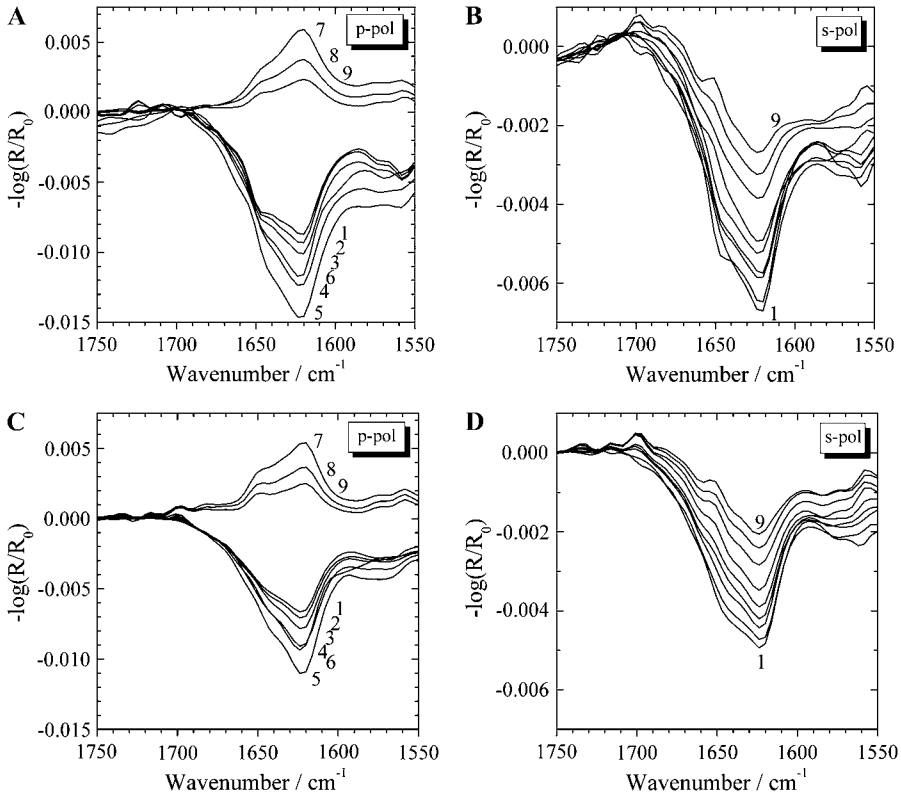

FIGURE 5 (*A*,*B*) IRRA spectra of HFar-N-Ras (200 nM) adsorbed at the air-D_2O interface acquired with p- (*A*) and s-polarized (*B*) light at various incident angles: *1*, 32°; *2*, 36°; *3*, 40°; *4*, 44°; *5*, 48°; *6*, 52°; *7*, 60°; *8*, 64°; and *9*, 68°. The surface pressure was 20 mN/m. (*C*,*D*) IRRA spectra of DH-N-Ras (200 nM) acquired under the same conditions as for panels *A* and *B*, at a surface pressure of 22 mN/m.

assumed that during the acquisition of the IRRA spectra the film did not evolve.

For our investigations, we used the same approach. We simulated amide-I band contours for s- and p-polarized light at different angles of the incident light, ranging from 32 to 68°, for the α-helical and β-sheet structures in the truncated H-Ras P21 protein, taking into account the different relative orientations of the secondary structure elements as obtained from the protein crystal structure of the truncated H-Ras protein P21. For the two secondary structure elements, a Lorentzian band shape with a reduced half-width of only 18 cm^{-1} was assumed to increase the separation and hence distinction of the bands located at 1650 cm^{-1} for the α-helix and 1620 cm^{-1} for the β-sheet, respectively. The different orientations for the α-helical and β-sheet structure elements relative to the air-D_2O interface were weighted according to the number of amino acids in the elements, and then averaged amide-I bands were simulated for the four proposed orientations *A–D* (see Fig. 4) of the total protein. In the simulation, a uniaxial distribution of the secondary structures relative to the surface normal to the air-D_2O interface was assumed. The amide-I band of an α-helix has two transition moments, the major one almost parallel to the long axis of the helix with an angle of ~36° relative to the helix axis and the degenerated one perpendicular to it. Since the second transition has the same frequency but much lower intensity, we used only the major transition for our calculations. Considering the uniaxial symmetry of the helix, no twist angle has to be taken into account for the simulations (see Fig. 6 *A*). For the β-sheet structure, the transition dipole moment of the amide-I mode is oriented along the interchain hydrogen bonds perpendicular to the strands (see Fig. 6 *B*). We now performed a detailed analysis of the tilt- and twist-angles Θ and Ψ for the secondary structure units of N-Ras using the x-ray structure as shown in Fig. 4. The values for Θ and Ψ and the different weighting factors are shown in Table 1 for the five α-helices and in Table 2 for the six strands of the β-sheet structure. The insertion of a value of 54.7° for Θ and 45° for Ψ into the spectral calculation corresponds to a random orientation of the vibrational dipole moments (see Tables 1 and 2). Because the vibrational dipole moments in an α-helix have a uniaxial distribution around the helix axis, Ψ was set 45° for all α-helical elements.

Fig. 7 shows simulated IRRA spectra for the protein orientations *A–D* at different angles of incidence and p- and s-polarized light. The simulated spectra look quite different compared to the experimental spectra due to the narrow bands assumed in the simulation. However, this facilitates the analysis as the intensity changes of the two bands due to the α-helix and the β-sheet structure can be seen more easily.

Comparison of the experimental (see Fig. 3) and simulated spectra (see Fig. 7) reveals that orientations *C* and *D* can be excluded for both N-Ras proteins. For orientation *D* very weak intensities are calculated and for orientation *C* the relative intensities of the two band components do not agree very well with the experimental spectra. It appears as if

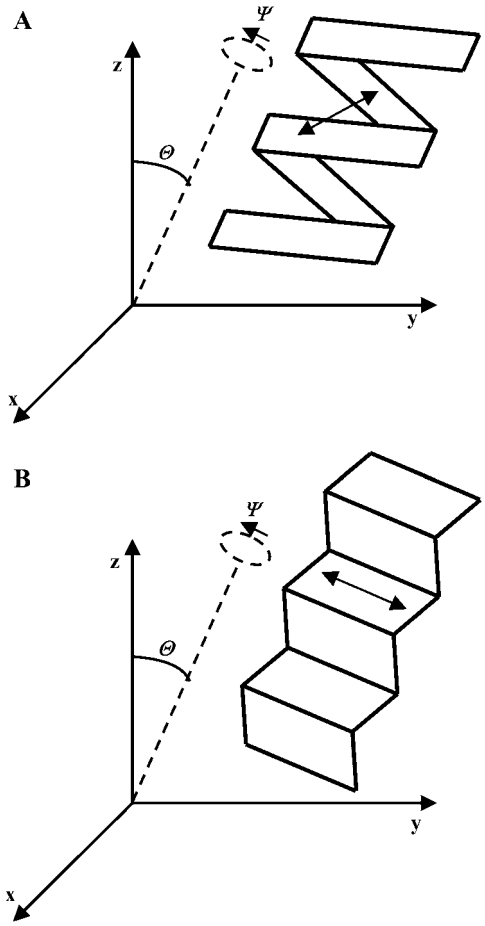

FIGURE 6 Schematic representation of an α-helix (*A*) and a β-sheet (*B*) in the molecular coordinate system. Euler angles Θ (*tilt angle*) and Ψ (*twist angle*) are indicated and the double-headed arrows describe the direction of the transition dipole moments in the α-helix (*A*) and β-sheets (*B*).

HFar-N-Ras is adsorbed at the air-D_2O interface directly with orientation *A*, whereas DH-N-Ras at lower surface pressure seems to be first adsorbed in a more random orientation at the interface (orientation *B*). With increasing pressure and higher surface coverage the protein then changes its orientation to orientation *A*. This interpretation is based on the observation that during the adsorption process the apparent maximum of the amide-I band shifts to lower wavenumber. This fact by itself already indicates that a change in orientation of the secondary structural elements of N-Ras with respect to the air-D_2O interface takes place. The comparison of experimental (see Fig. 5) and simulated angle-dependent spectra (see Fig. 7) support our hypothesis. For orientation *B*, the intensity of the high frequency band is higher at an angle of incidence of 40° for s-polarized light (see Fig. 7 *B*), and this corresponds to spectra *1* and *2* in Fig. 3 *D*. For orientation *A*, the intensity of the low frequency band is higher for s-polarized light (Fig. 7 *A*) and this agrees with the experimental spectra *4* and *5* in Fig. 3 *D*, and *2* and *3* in Fig. 3 *B*. We therefore conclude that at the saturation pressure both N-Ras proteins are adsorbed at the air-D_2O interface in the same way corresponding to the orientation *A* in Fig. 4. However, DH-N-Ras is adsorbed with different kinetics, because at low surface pressure it is first adsorbed in a more random orientation.

When the simulated spectra at different angles are compared with the experimental spectra shown in Fig. 5 obtained at the saturation pressure, it is clear that only orientation *A* gives simulated spectra with the intensity of the low frequency band being always higher at all angles of incidence as observed and changing its sign at the Brewster angle when p-polarized light is used.

TABLE 1 Tilt-angle Θ for the α-helices

Secondary structure	Θ (*A*)	Θ (*B*)	Θ (*C*)	Θ (*D*)
α1	10 × 15°	10 × 54.7°	10 × 60°	10 × 60°
α2	10 × 15°	10 × 54.7°	10 × 30°	10 × 75°
α3	17 × 55°	17 × 54.7°	17 × 80°	17 × 10°
α4	11 × 45°	11 × 54.7°	11 × 90°	11 × 0°
α5	13 × 45°	13 × 54.7°	13 × 90°	13 × 0°

Tilt-angle Θ for the α-helices α1 (residues 16–25), α2 (residues 65–74), α3 (residues 87–103), α4 (residues 127–137), and α5 (residues 152–164) of truncated H-Ras P21 (PDB entry 121p) for different orientations (*A–D*) relative to the normal of the air-D_2O interface. The different orientations for the α-helical structure elements relative to the air-D_2O interface were weighted according to the number of amino acids in the elements. The value of 54.7° for Θ corresponds to a random orientation of the vibrational dipole moments.

TABLE 2 Tilt-angle Θ and twist-angle Ψ

Secondary structure	Θ (*A*)	Θ (*C*)	Θ (*D*)	Ψ (*A,C,D*)	Θ (*B*)	Ψ (*B*)
β1	5 × 25°	5 × 70°	5 × 20°	5 × 0°	5 × 54.7°	5 × 45°
	3 × 25°	3 × 70°	3 × 20°	3 × 45°	3 × 54.7°	3 × 45°
	2 × 25°	2 × 70°	2 × 20°	2 × 90°	2 × 54.7°	2 × 45°
β2	2 × 45°	2 × 0°	2 × 90°	2 × 45°	2 × 54.7°	2 × 45°
	8 × 0°	8 × 45°	8 × 45°	8 × 45°	8 × 54.7°	8 × 45°
β3	2 × 45°	2 × 0°	2 × 90°	2 × 45°	2 × 54.7°	2 × 45°
	6 × 10°	6 × 55°	6 × 35°	6 × 0°	6 × 54.7°	6 × 45°
β4	5 × 45°	5 × 90°	5 × 0°	5 × 90°	5 × 54.7°	5 × 45°
	2 × 0°	2 × 45°	2 × 45°	2 × 45°	2 × 54.7°	2 × 45°
β5	4 × 45°	4 × 90°	4 × 0°	4 × 90°	4 × 54.7°	4 × 45°
	2 × 45°	2 × 90°	2 × 0°	2 × 45°	2 × 54.7°	2 × 45°
β6	3 × 25°	3 × 70°	3 × 20°	3 × 90°	3 × 54.7°	3 × 45°

Tilt-angle Θ and twist-angle Ψ for the six strands of the β-sheet β1 (residues 37–46), β2 (residues 49–58), β3 (residues 2–9), β4 (residues 77–83), β5 (residues 111–116), and β6 (residues 141—143) of truncated H-Ras P21 (PDB entry 121p) for different orientations (*A–D*) relative to the normal of the air-D_2O interface. The different orientations for the β-sheet structure elements relative to the air-D_2O interface were weighted according to the number of amino acids in the elements. The values of 54.7° for Θ and 45° for Ψ correspond to a random orientation of the vibrational dipole moments.

Insertion of N-Ras proteins into ternary lipid mixtures

We first investigated the insertion of HFar-N-Ras into a POPC/BSM/Chol lipid film at constant surface pressure. The

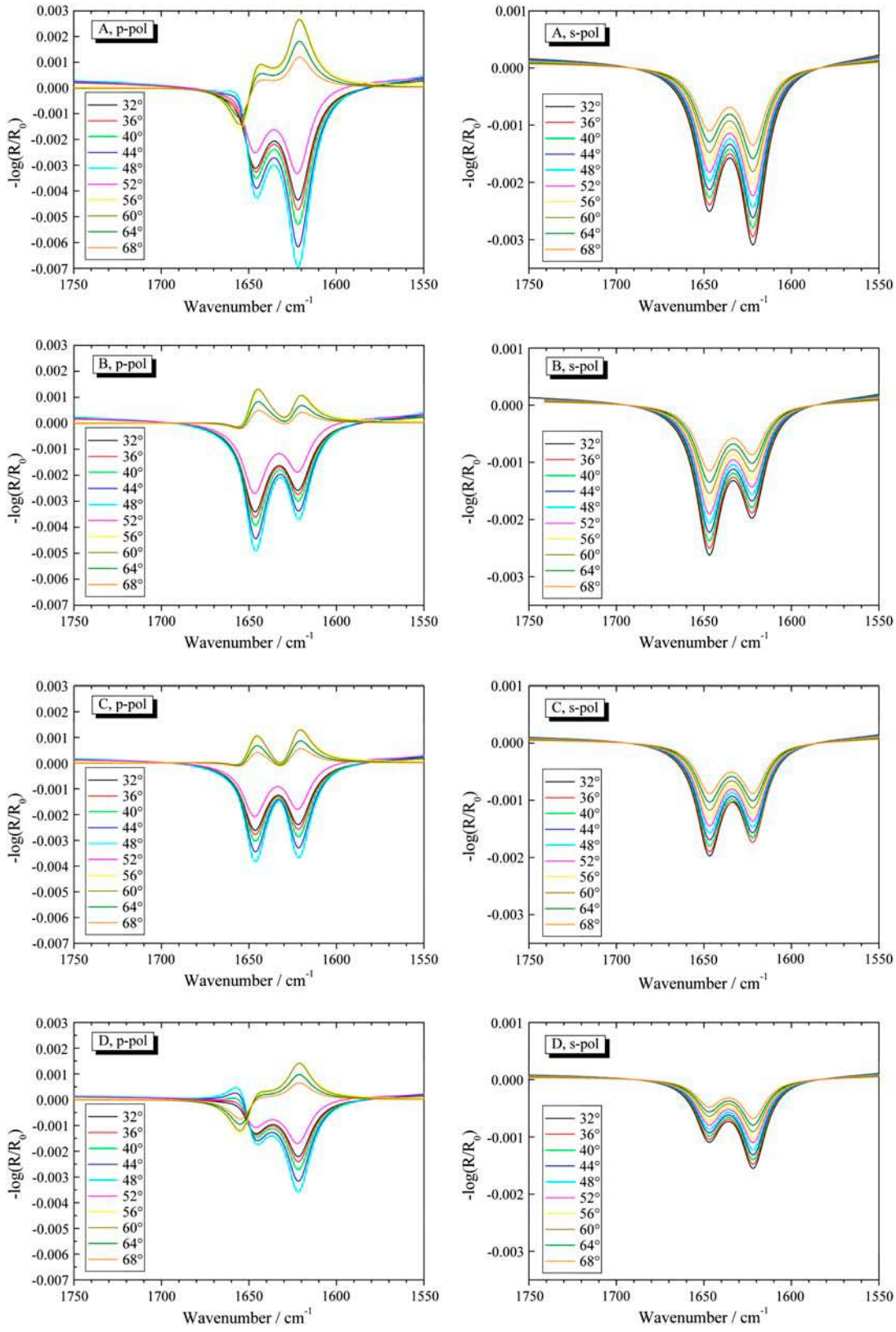

FIGURE 7 Simulated IRRA spectra of α-helical and β-sheet elements of the Ras protein occupying the orientations *A–D* relative to the normal of the air-D_2O interface. The calculations were performed for p- and s-polarized light and for different angles of incidence: *1*, 32°; *2*, 36°; *3*, 40°; *4*, 44°; *5*, 48°; *6*, 52°; *7*, 56°; *8*, 60°; *9*, 64°; and 10, 68° for the amide-I band.

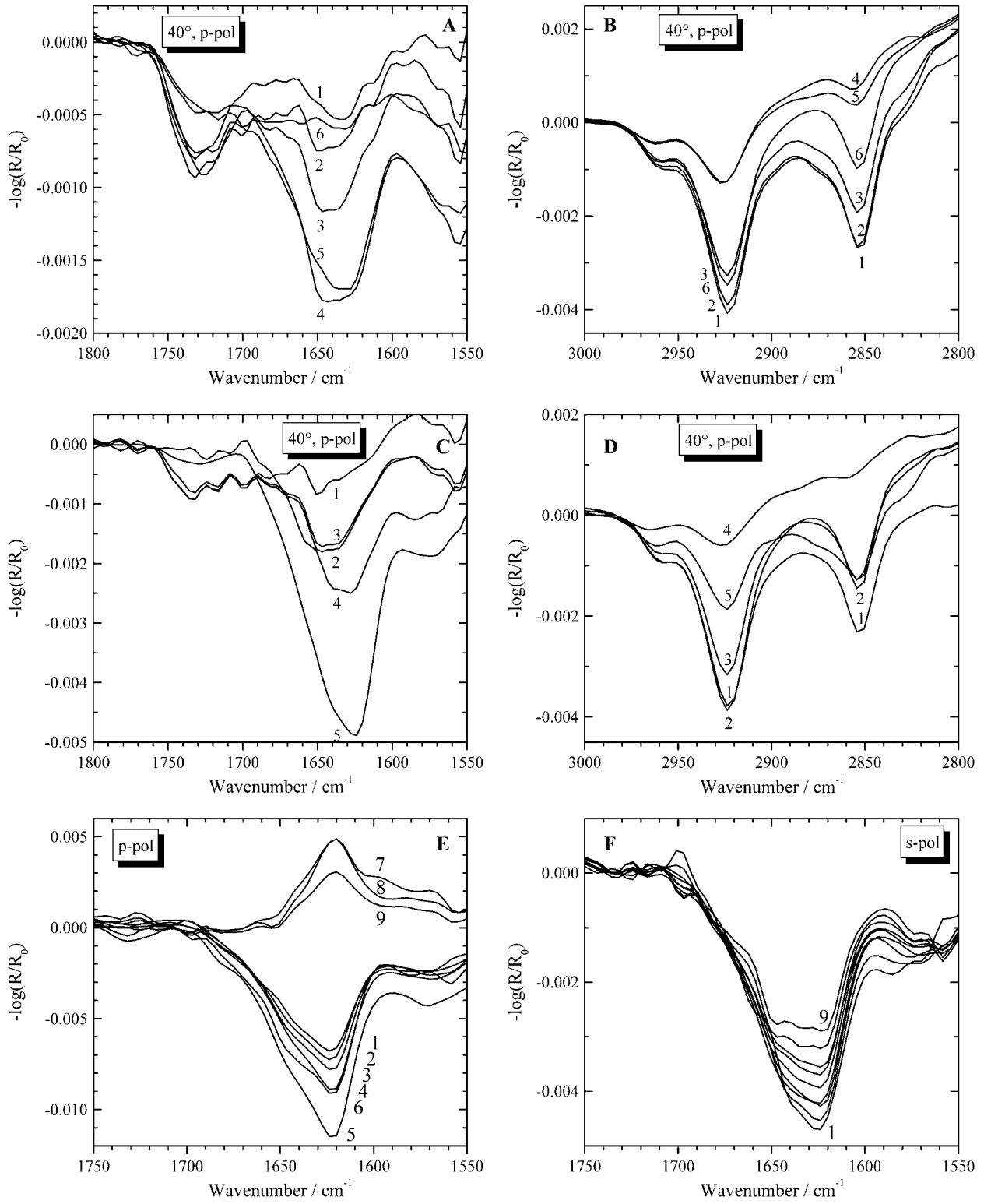

FIGURE 8 (*A*) IRRA spectra of the amide-I region for POPC/BSM/Chol monolayer at 30 mN/m on D_2O (100 mM NaCl; curve *1*), 2 h after injection of HFar-N-Ras at 30 mN/m (400 nM; curve *2*), 1 h after injection of the protein at 20 mN/m (600 nM; curve *3*), 3 h after relaxation to 10 mN/m (curve *4*), 4 h after relaxation to 10 mN/m (curve *5*), and 2 h after recompression to 30 mN/m (curve *6*). The spectra were acquired using p-polarized light at an angle of incidence of 40°. (*B*) IRRA spectra of the CH_2 stretching region (*1–6*) taken at the same conditions as for panel *A*. (*C*) IRRA spectra of the amide-I region for POPC/BSM/Chol monolayer at 30 mN/m on D_2O (100 mM NaCl; curve *1*), 2 h after injection of DH-N-Ras at 30 mN/m (400 nM; curve *2*), 1 h after relaxation to 20 mN/m (curve *3*), 2 h after relaxation to 10 mN/m (curve *4*), and 1 h after recompression to 30 mN/m (curve *5*). (*D*) IRRA spectra of the CH_2 stretching region (*1–5*) taken at the same conditions as for panel *C*. The spectra were acquired using p-polarized light at an angle of incidence of 40°. (*E*,*F*) IRRA spectra of

lipid mixture was spread onto the air-D_2O interface and the film was compressed to a surface pressure of 30 mN/m, a pressure value where the monolayer has a similar lipid density as found in lipid bilayers. The spectrum of the lipid film shows a weak amide-I band at 1635 cm^{-1} originating from the amide group of the sphingomyelin (Fig. 8 *A*, spectrum *1*). The band at 1735 cm^{-1} is due to the C=O groups of the POPC. We then injected a concentrated protein solution underneath the monolayer using a syringe to obtain a subphase concentration of 400 nM. Two hours after the injection no change in area per molecule at constant pressure was observed but the amide-I band intensity increased slightly, indicating a beginning adsorption of the protein. Because the molecular area at constant pressure did not change, one could possibly conclude that the protein does not insert into the lipid monolayer (see Fig. 8 *A*, spectrum *2*). However, when the number of protein molecules is approximated from the band-intensity increase (~0.00025 absorbance units), one comes to the conclusion that only one protein per 500 lipid molecules is at the interface, i.e., the area should change by 0.2% only. This is definitely outside the detection limit. We suggest therefore, that the protein is indeed incorporated into the lipid monolayer with its acyl chains, though it is not apparent from the area change. After expansion of the film to obtain a surface pressure of 20 mN/m and additional injections of the protein to obtain a 600 nM subphase concentration, the amide-I intensity increased by a factor of ~2 (Fig 8 *A*, spectrum *3*). Again, no significant change in area at constant pressure was detected, probably because of the same reasons mentioned above. We then expanded the film to obtain a pressure of 10 mN/m. After a waiting time of 3–4 h, a large increase of the area per molecule at constant pressure (not shown) to twice its original value was observed. Apparently, at a pressure of 10 mN/m the protein was now able to insert into the lipid monolayer and reach the air-D_2O interface. This was also evident from the much larger increase in intensity of the amide-I band (Fig. 8 *A*, spectrum *4*). Concomitantly, the band maximum shifted slightly to 1632 cm^{-1}, which indicates a reorientation of the protein when inserted in between the lipids at the air-D_2O interface (Fig. 8 *A*, spectrum *5*).

After a recompression of the monolayer to 30 mN/m, the additional amide-I band intensity due to the protein insertion could not be detected any more, indicating a more or less complete squeeze-out of the protein from the lipid monolayer (Fig. 8 *A*, spectrum *6*). Obviously, the protein was not inserted into the lipid monolayer in a stable fashion, indicating that the two anchors, one farnesyl and one hexadecyl, provide not enough gain in free energy that the protein remains incorporated in the monolayer at higher surface pressure.

In Fig. 8 *B*, the antisymmetric and symmetric CH_2 stretching vibrational bands are shown. Due to their conformational sensitivity, these modes can be empirically correlated with the *trans*/*gauche* ratio of the alkyl chains. The frequencies of the band maxima at 2924 cm^{-1} and 2854 cm^{-1}, respectively, are not affected by the incorporation of the protein. The experimental frequencies are characteristic of disordered alkyl chains with a high amount of *gauche* conformers, i.e., an essentially liquid-expanded state of the monolayer at all surface pressures. The intensity of both modes decreases with decreasing surface pressure and after recompression and squeeze-out of the protein, 80–90% of the original intensity is obtained.

IRRAS is not suited to obtain information on possible domain formation in lipid monolayers. The cross-section of the IRRAS beam extends over ~1 cm^2, depending on the angle of the incident light, whereas POPC/BSM/Chol domains have a size from several nanometers up to the μm range (16), so that the IRRA spectra provide only an averaged information about the alkyl-chain conformation.

We used a similar experimental procedure to study the interaction of the doubly hexadecylated DH-N-Ras with POPC/BSM/Chol monolayers (Fig. 8, *C* and *D*). After compression of the lipid film to 30 mN/m and injection of the protein (bulk concentration 400 nM), no significant change in area per molecule at constant pressure was observed. However, the amide-I band intensity increased by 0.001 absorbance units, which means that ~1 protein per 150 lipid molecules is now at the interface (spectrum *2*). The band maximum appeared again at 1647 cm^{-1}, indicating a more random orientation of the protein in the lipid monolayer (see Figs. 4 *B* and 7 *B*). A similar band was observed after expansion of the film to a pressure of 20 mN/m, i.e., no further increase in protein concentration at the interface was observed (spectrum *3*). In contrast to the experiment with HFar-N-Ras no additional injection was done, so the bulk protein concentration was constant at 400 nM. Further expansion of the film to 10 mN/m showed after 2 h a large increase of the area per molecule at constant pressure (not shown), induced by the accumulation of the protein at the air-D_2O interface between the lipid molecules. At the same time, the amide-I band intensity increased by a factor of 2 and its maximum shifted to 1628 cm^{-1} (spectrum *4*), which indicates a reorientation of the protein from the random orientation to orientation *A* (see Fig. 4).

We now recompressed the film to 30 mN/m. In this case, an additional strong increase of the amide-I band and a further shift of the band maximum to 1625 cm^{-1} were seen. This indicates that the doubly-hexadecylated protein DH-N-Ras remains inserted in between the lipid molecules in the

FIGURE 8 (Continued).

DH-N-Ras (400 nM) adsorbed at the lipid interface acquired with p- (*E*) and s-polarized (*F*) light at various incident angles: *1*, 32°; *2*, 36°; *3*, 40°; *4*, 44°; *5*, 48°; *6*, 52°; *7*, 60°; *8*, 64°; and *9*, 68°. The surface pressure was 30 mN/m.

monolayer and that some protein molecules are in contact with air. The CH_2-bands provide additional information for this assumption. Expansion to 10 mN/m decreases their intensity as expected. Recompression to 30 mN/m, however, does not lead to almost the same band intensity as in the case of HFar-N-Ras, which is squeezed-out, but to a reduced intensity of ~50% (Fig. 8 *D*, spectrum *5*). This indicates that some of the area at the air-D_2O interface is occupied by the protein and by the lipid anchors. However, the intensity of the amide-I band after recompression (see Fig. 8 *C*, spectrum *5*) is only 30% lower as for the pure protein film (see Fig. 5 *C*, spectrum *3*), namely ~0.005 absorbance units. This means that we have a layer of proteins at the interface with somewhat reduced density compared to the pure protein film. Some of the proteins have to be located beneath the lipid headgroups of the monolayer and the other part is probably inserted into the chain region. The comparison of experimental (see Fig. 8, *E* and *F*) and simulated angle-dependent spectra (see Fig. 7) shows that, overall, the protein is oriented in the same fashion as when it is adsorbed at the air-D_2O interface. The amide-I band intensity ratios for α-helical and β-sheet contributions calculated for different angles are in general agreement for experimental and calculated spectra.

In a second series of experiments, we investigated the insertion of N-Ras proteins into POPC/BSM/Chol monolayers at constant surface area starting from low surface pressure of the lipid monolayer. In this experiment we wanted to see which surface pressure would be reached by the incorporation of the protein into the lipid film. The lipid mixture was spread onto the air-D_2O interface until a surface pressure of ~10 mN/m was reached. Then the protein was injected to obtain a 200 nM protein subphase concentration. We then recorded the surface pressure as a function of time. Fig. 9, *A* and *C*, show the surface-pressure versus time-course for the insertion of HFar-N-Ras and DH-N-Ras, respectively, into the lipid monolayer. Whereas the surface pressure increases continuously for HFar-N-Ras up to 29 mN/m, a short plateau is observed for DH-N-Ras at 18 mN/m before the final surface pressure of 25 mN/m is reached. Similar differences were observed for the adsorption of the two different proteins at the air-D_2O interface (see Fig. 2).

Fig. 9, *B* and *D*, show the IRRA spectra taken at times as indicated. They show amide-I bands with a frequency maximum of 1624 cm^{-1}, indicating a preferred insertion of HFar-N-Ras in orientation *A*. In spectrum *1*, the band edge of the HOD bending mode of the subphase is discernible. In the reference trough a rapid H-D exchange due to the H_2O vapor above the D_2O surface occurs after the trough has been covered with the hood. This exchange is slower for the sample trough due to lipid film acting as a barrier for water exchange and leads to the appearance of a positive uncompensated HOD band. However, after several hours the H-D exchange has taken place also in the sample trough so that both troughs contain nearly equal amounts of HOD. As a consequence, the intensity of this HOD band decreases during the experiment until after several hours the HOD band is compensated.

According to the frequency shift of the amide-I bands from 1635 to 1624 cm^{-1}, indicated in Fig. 9 *D*, the insertion of DH-N-Ras into the lipid monolayer starts in a random way up to the first small surface pressure plateau and ends up in orientation *A* at the final surface pressure plateau. Angle-dependent measurements are given in Fig. 9, *E* and *F*, which show for orientation *A* the characteristic course of the reflectance-absorbance values.

SUMMARY AND CONCLUSIONS

The adsorption and orientation of two different N-Ras proteins, namely a farnesylated and hexadecylated (HFar-N-Ras) and a doubly-hexadecylated (DH-N-Ras) N-Ras protein, respectively, at the air-D_2O interface were investigated using infrared reflection absorption spectroscopy (IRRAS). In a second series of experiments the insertion of these proteins into a lipid monolayer (POPC/BSM/Chol) was studied. Both proteins are surface-active and form a Gibbs monolayer at the air-D_2O interface. Significant differences in IRRA band contours were observed due to differences in the orientation of the N-Ras proteins as a consequence of their different lipidation patterns. Both N-Ras proteins adsorb at the air-D_2O interface in the same way, corresponding to orientation *A* in Fig. 4. The DH-N-Ras adsorbs with a different kinetics, however, and at low surface pressures it is first adsorbed in a more random orientation.

Langmuir monolayers of the lipid mixture POPC/BSM/Chol (2:1:1) were used as half of a model raft lipid bilayer system to study the insertion of the two doubly-lipidated N-Ras proteins. Both proteins insert with their lipid anchors into the lipid monolayer but at higher surface pressures (30 mN/m), the farnesylated and hexadecylated protein desorbs almost completely from the monolayer, whereas the doubly hexadecylated protein remains incorporated into the lipid monolayer, indicating a higher gain in free energy for insertion for the doubly-hexadecylated protein. During the insertion process, changes in the orientation of the protein were detected by comparison with simulated IRRA spectra, which were based on the information on the relative orientation of the secondary structure elements obtained from the protein crystal structure data. The comparison of experimental and simulated angle-dependent IRRA spectra reveals a preferred insertion of HFar-N-Ras in orientation A. The doubly-hexadecylated protein DH-N-Ras remains inserted in between the lipid molecules in the monolayer even at high surface pressures. Such a different behavior would be in line with the lower affinity of short and unsaturated chains in liquid-ordered phases and the finding that farnesylation alone is insufficient to stably anchor the Ras protein to the plasma membrane (50,51).

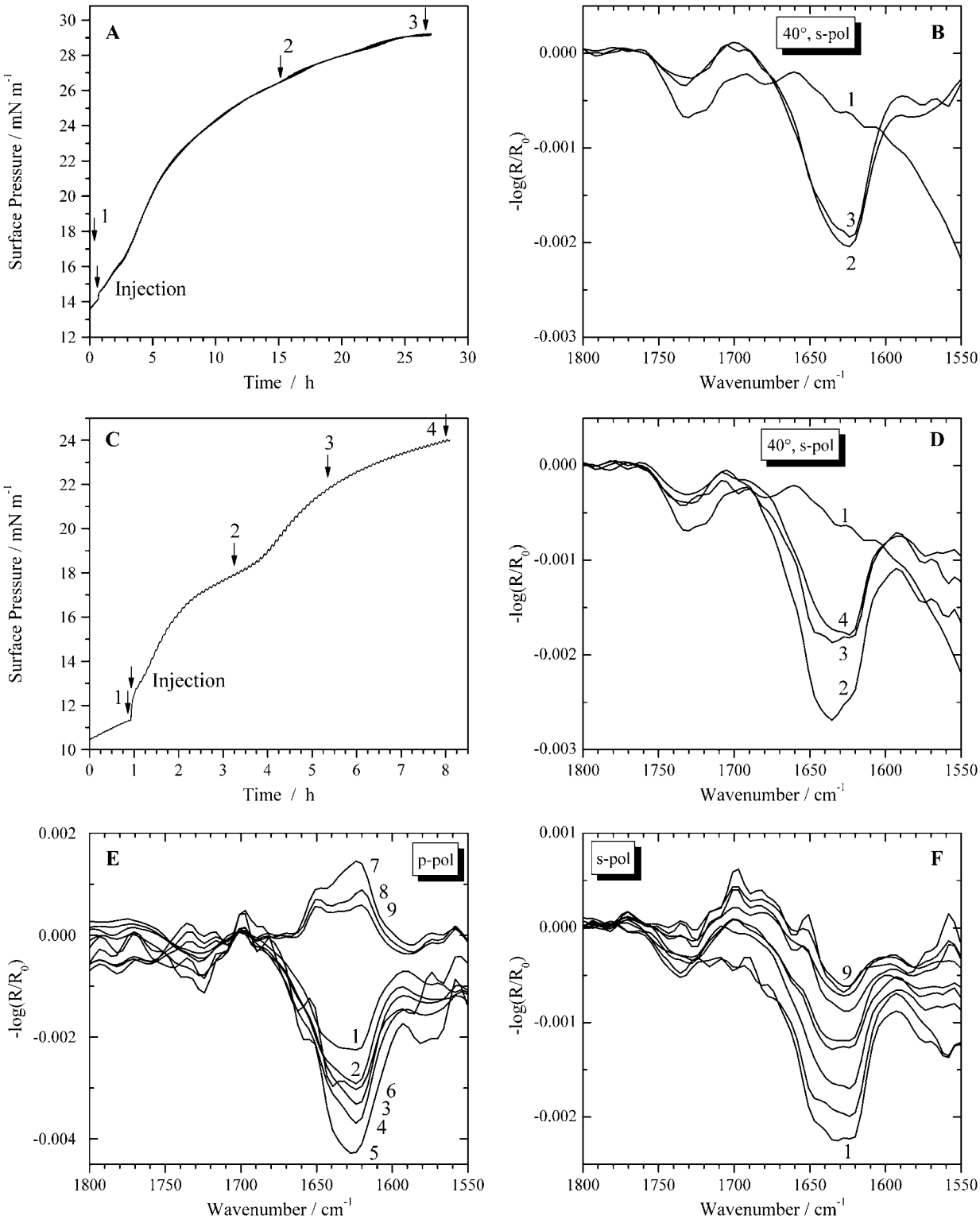

FIGURE 9 (*A*) Surface-pressure versus time-course of a POPC/BSM/Chol film after injection of HFar-N-Ras (200 nM). (*B*) IRRA spectra of the lipid film (*1*) at 13.5 mN/m and mixed lipid/protein films (*2*,*3*) at the respective positions of the surface-pressure versus time-curve in panel *A*. All spectra were recorded with an angle of incidence of 40° with s-polarized light. (*C*) Surface-pressure versus time-course of a POPC/BSM/Chol film after injection of DH-N-Ras (200 nM). (*D*) IRRA spectra of the lipid film (*1*) at 11.5 mN/m and mixed lipid/protein films (*2–4*) at the respective positions of the surface-pressure time-curve in panel *C*. All spectra were recorded at an angle of incidence of 40° with s-polarized light. (*E*,*F*) IRRA spectra of DH-N-Ras (400 nM) adsorbed at the lipid interface acquired with p- (*E*) and s-polarized (*F*) light at various incident angles: *1*, 32°; *2*, 36°; *3*, 40°; *4*, 44°; *5*, 48°; *6*, 52°; *7*, 60°; *8*, 64°; and *9*, 68°. The surface pressure was 25 mN/m.

Financial support from the Deutsche Forschungsgemeinschaft (grant No. SFB 642) to R.W., H.W., and J.K., and grant No. Bl 182/19-1 to A.M. and A.B. and the Fonds der Chemischen Industrie, is gratefully acknowledged.

REFERENCES

1. Reuther, G. W., and C. J. Der. 2000. The Ras branch of small GTPases: Ras family members don't fall far from the tree. *Curr. Opin. Cell Biol.* 12:157–165.
2. Campbell, S. L., R. Khosravi-Far, K. L. Rossman, G. J. Clark, and C. J. Der. 1998. Increasing complexity of Ras signaling. *Oncogene.* 17: 1395–1413.
3. Wittinghofer, A., and H. Waldmann. 2000. Ras—a molecular switch involved in tumor formation. *Angew. Chem. Int. Ed. Engl.* 39:4192–4214.
4. Hancock, J. F. 2003. Ras proteins: different signals from different locations. *Nat. Rev. Mol. Cell Biol.* 4:373–383.
5. Casey, P. J., P. A. Solski, C. J. Der, and J. E. Buss. 1989. p21Ras is modified by a farnesyl isoprenoid. *Proc. Natl. Acad. Sci. USA.* 86: 8323–8327.
6. Lobo, S., W. K. Greentree, M. E. Lindner, and R. J. Deschenes. 2002. Identification of a Ras palmitoyltransferase in *Saccharomyces cerevisiae*. *J. Biol. Chem.* 277:41268–41273.
7. Zhang, F. L., and P. J. Casey. 1996. Protein prenylation: molecular mechanisms and functional consequences. *Annu. Rev. Biochem.* 65: 241–269.
8. Hancock, J. F., A. I. Magee, J. E. Childs, and C. J. Marshall. 1989. All Ras proteins are polyisoprenylated but only some are palmitoylated. *Cell.* 57:1167–1177.
9. Hancock, J. F., K. Cadwallader, and C. J. Marshall. 1991. Methylation and proteolysis are essential for efficient membrane binding of prenylated p21K-Ras(B). *EMBO J.* 10:641–646.
10. Schroeder, H., R. Leventis, S. Rex, M. Schelhaas, E. Nägele, H. Waldmann, and J. R. Silvius. 1997. S-Acylation and plasma membrane targeting of the farnesylated carboxyl-terminal peptide of N-Ras in mammalian fibroblasts. *Biochemistry.* 36:13102–13109.
11. Huster, D., K. Kuhn, D. Kadereit, H. Waldmann, and K. Arnold. 2001. ^{1}H high-resolution magic angle spinning NMR spectroscopy for the investigation of a Ras lipopeptide in a lipid membrane. *Angew. Chem. Int. Ed. Engl.* 40:1056–1058.
12. Huster, D., A. Vogel, C. Katzka, H. A. Scheidt, H. Binder, S. Dante, T. Gutberlet, O. Zschörnig, H. Waldmann, and K. Arnold. 2003. Membrane insertion of a lipidated Ras peptide studied by FTIR, solid-state NMR, and neutron diffraction spectroscopy. *J. Am. Chem. Soc.* 125:4070–4079.
13. Janosch, S., C. Nicolini, B. Ludolph, C. Peters, M. Völkert, T. L. Hazlet, T. E. Gratton, H. Waldmann, and R. Winter. 2004. Partitioning of dual-lipidated peptides into membrane microdomains: lipid sorting vs. peptide aggregation. *J. Am. Chem. Soc.* 126:7496–7503.
14. Vogel, A., C. P. Katzka, H. Waldmann, K. Arnold, M. F. Brown, and D. Huster. 2005. Lipid modifications of a Ras peptide exhibit altered packing and mobility versus host membrane as detected by ^{2}H solid-state NMR. *J. Am. Chem. Soc.* 127:12263–12272.
15. Bader, B., K. Kuhn, D. J. Owen, H. Waldmann, A. Wittinghofer, and J. Kuhlmann. 2000. Bioorganic synthesis of lipid-modified proteins for the study of signal transduction. *Nature.* 403:223–226.
16. Nicolini, C., J. Baranski, S. Schlummer, J. Palomo, M. Lumbierres-Burgues, M. Kahms, J. Kuhlmann, S. Sanchez, E. Gratton, H. Waldmann, and R. Winter. 2006. Visualizing association of N-Ras in lipid microdomains: influence of domain structure and interfacial adsorption. *J. Am. Chem. Soc.* 128:192–201.
17. Giehl, A., T. Lemm, O. Bartelsen, K. Sandhoff, and A. Blume. 1999. Interaction of the GM2-activator protein with phospholipid-ganglioside bilayer membranes and with monolayers at the air-water interface. *Eur. J. Biochem.* 261:650–658.
18. Hanakam, F., G. Gerisch, S. Lotz, T. Alt, and A. Seelig. 1996. Binding of hisactophilin I and II to lipid membranes is controlled by a pH-dependent myristoyl-histidine switch. *Biochemistry.* 35:11036–11044.
19. Seitz, H. R., M. Heck, K. P. Hofmann, T. Alt, J. Pellaud, and A. Seelig. 1999. Molecular determinants of the reversible membrane anchorage of the G-protein transducin. *Biochemistry.* 38:7950–7960.
20. Ege, C., J. Majewski, G. Wu, K. Kjaer, and K. Y. C. Lee. 2005. Templating effect of lipid membranes on Alzheimer's amyloid β-peptide. *ChemPhysChem.* 6:226–229.
21. Spaar, A., C. Münster, and T. Salditt. 2004. Conformation of peptides in lipid membranes studied by x-ray grazing incidence scattering. *Biophys. J.* 87:396–407.
22. Maltseva, E., and G. Brezesinski. 2004. Adsorption of amyloid β (1–40) peptide to phosphatidylethanolamine monolayers. *ChemPhys Chem.* 5:1185–1190.
23. Maltseva, E., A. Kerth, A. Blume, H. Möhwald, and G. Brezesinski. 2005. Adsorption of amyloid β (1–40) peptide at phospholipid monolayers. *ChemBioChem.* 6:1817–1824.
24. Vacklin, H. P., F. Tiberg, G. Fragneto, and R. K. Thomas. 2005. Phospholipase A2 hydrolysis of supported phospholipid bilayers: a neutron reflectivity and ellipsometry study. *Biochemistry.* 44:2811–2821.
25. Malkova, S., F. Long, R. V. Stahelin, S. V. Pingali, D. Murray, W. Cho, and M. L. Schlossman. 2005. X-ray reflectivity studies of cPLA2α-C2 domains adsorbed onto Langmuir monolayers of SOPC. *Biophys. J.* 89:1861–1873.
26. Pastrana-Rios, B., S. Taneva, K. M. W. Keough, A. J. Mautone, and R. Mendelsohn. 1995. External reflection absorption infrared spectroscopy study of lung surfactant proteins SP-B and SP-C in phospholipid monolayers at the air/water interface. *Biophys. J.* 69: 2531–2540.
27. Castano, S., and B. Desbat. 2005. Structure and orientation study of fusion peptide FP23 of gp41 from HIV-1 alone or inserted into various lipid membrane models (mono-, bi- and multibilayers) by FT-IR spectroscopies and Brewster angle microscopy. *Biochim. Biophys. Acta.* 1715:81–95.
28. Wang, L., P. Cai, H.-J. Galla, H. He, C. R. Flach, and R. Mendelsohn. 2005. Monolayer-multilayer transitions in a lung surfactant model: IR reflection-absorption spectroscopy and atomic force microscopy. *Eur. Biophys. J.* 34:243–254.
29. Kota, Z., T. Pali, and D. Marsh. 2004. Orientation and lipid-peptide interactions of gramicidin A in lipid membranes: polarized attenuated total reflection infrared spectroscopy and spin-label electron spin resonance. *Biophys. J.* 86:1521–1531.
30. Xu, Z., J. W. Brauner, C. R. Flach, and R. Mendelsohn. 2004. Orientation of peptides in aqueous monolayer films. Infrared reflection-absorption spectroscopy studies of a synthetic amphipathic β-sheet. *Langmuir.* 20:3730–3733.
31. Lad, M. D., F. Birembaut, R. A. Frazier, and R. Green. 2005. Protein-lipid interactions at the air/water interface. *J. Phys. Chem. Chem. Phys.* 7:3478–3485.
32. Reents, R., M. Wagner, S. Schlummer, J. Kuhlmann, and H. Waldmann. 2005. Synthesis and application of fluorescent Ras proteins for live-cell imaging. *ChemBioChem.* 6:86–94.
33. Wagner, M., and J. Kuhlmann. 2004. Generation and characterization of Ras lipoproteins based on chemical coupling. *Methods Mol. Biol. Bioconjug. Protocols.* 283:245–254.
34. Flach, C. R., J. W. Brauner, J. W. Taylor, R. C. Baldwin, and R. Mendelsohn. 1994. External reflection FTIR of peptide monolayer films at the air/water interface: experimental design, spectra-structure correlations, and effects of hydrogen-deuterium exchange. *Biophys. J.* 67:402–410.
35. Mendelsohn, R., J. W. Brauner, and A. Gericke. 1995. External infrared reflection absorption spectrometry of monolayer films at the air-water interface. *Annu. Rev. Phys. Chem.* 46:305–334.

36. Flach, C. R., A. Gericke, and R. Mendelsohn. 1997. Quantitative determination of molecular tilt angles in monolayer films at the air/water interface: infrared reflection/absorption spectroscopy of behenic acid methyl ester. *J. Phys. Chem. B.* 101:58–65.

37. Wittinghofer, F., U. Krengel, J. John, W. Kabsch, and E. F. Pai. 1991. Three-dimensional structure of p21 in the active conformation and analysis of an oncogenic mutant. *Environ. Health Perspect.* 93: 11–15.

38. Kerth, A., A. Erbe, M. Dathe, and A. Blume. 2004. Infrared reflection absorption spectroscopy of amphipathic model peptides at the air/water interface. *Biophys. J.* 86:3750–3758.

39. Vermeer, A. W. P. 2002. Conformation of adsorbed proteins. *In* Encyclopedia of Surface and Colloid Science, Vol. 1. A.T. Hubbard, editor. Marcel Dekker, New York. 1193–1212.

40. Bos, M. A., and T. Nylander. 1996. Interaction between β-lactoglobulin and phospholipids at the air/water interface. *Langmuir.* 12:2791–2797.

41. Chirgadze, Y. N., and N. A. Nevskaya. 1976. Infrared spectra and resonance interaction of amide-I vibration of the antiparallel-chain pleated sheet. *Biopolymers.* 15:607–625.

42. Wu, F., C. R. Flach, B. A. Seaton, T. R. Mealy, and R. Mendelsohn. 1999. Stability of annexin V in ternary complexes with Ca^{2+} and anionic phospholipids: IR studies of monolayer and bulk phases. *Biochemistry.* 38:792–799.

43. Cornut, I., B. Desbat, J. M. Turlet, and J. Dufourcq. 1996. In situ study by polarization modulated Fourier transform infrared spectroscopy of the structure and orientation of lipids and amphipathic peptides at the air-water interface. *Biophys. J.* 70:305–312.

44. Dluhy, R. A., S. Shanmukh, J. B. Leapard, P. Krüger, and J. E. Baatz. 2003. Deacylated pulmonary surfactant protein SP-C transforms from α-helical to amyloid fibril structure via a pH-dependent mechanism: an infrared structural investigation. *Biophys. J.* 85:2417–2429.

45. Blaudez, D., J.-M. Turlet, J. Dufourcq, D. Bard, T. Buffeteau, and B. Desbat. 1996. Investigations at the air/water interface using polarization modulation IR spectroscopy. *J. Chem. Soc. Faraday Trans.* 92: 525–530.

46. Gallant, J., B. Desbat, D. Vaknin, and C. Salesse. 1998. Polarization-modulated infrared spectroscopy and x-ray reflectivity of photosystem II core complex at the gas-water interface. *Biophys. J.* 75:2888–2899.

47. Ronzon, F., B. Desbat, T. Buffeteau, C. Mingotaud, J.-P. Chauvet, and B. Roux. 2002. Structure and orientation of a glycosylphosphatidyl inositol anchored protein at the air/water interface. *J. Phys. Chem.* 106:3307–3315.

48. Ulrich, W.-P., and H. Vogel. 1999. Polarization-modulated FTIR spectroscopy of lipid/gramicidin monolayers at the air/water interface. *Biophys. J.* 76:1639–1647.

49. Gericke, A., C. R. Flach, and R. Mendelsohn. 1997. Structure and orientation of lung surfactant SP-C and L-α -dipalmitoylphosphatidylcholine in aqueous monolayers. *Biophys. J.* 73:492–499.

50. Wang, T.-Y., R. Leventis, and J. R. Silvius. 2000. Fluorescence-based evaluation of the partitioning of lipids and lipidated peptides into liquid-ordered lipid microdomains: a model for molecular partitioning into ''lipid rafts''. *Biophys. J.* 79:919–933.

51. Hancock, J. E., and R. G. Parton. 2005. Ras plasma membrane signalling platforms. *Biochem. J.* 389:1–11.